EVALUATION OF WATER VAPOR DISTRIBUTION IN VERSIONS OF THE ECHAM MODEL USING SATELLITE OBSERVATION

C.-T. Chen

Max-Planck Institute for Meteorology
Hamburg, F. R. Germany

1. INTRODUCTION

Water vapor is the most important variable constituent of the Earth's atmosphere [Chahine, 1992]. Its distribution, transport, and convergence determine cloud formation and precipitation which affect the agriculture and other human activities. The transform of water in the various phases in hydrological cycle and their interactions with convection, large scale circulation and land surface processes are important for energy transfer in the earth-atmosphere system.Water vapor also profoundly modifies the radiative properties of the atmosphere. Water vapor is the primary greenhouse gas in the atmosphere. The longwave radiative cooling in the troposphere is mainly due to water vapor. Clouds, formed from condensation of water vapor, strongly regulate both the net incoming solar and out-going longwave radiation. In short, water vapor imposes strong influences on the climate variations on a variety of temporal and spatial scale. It is impossible to simulate the climate of the atmosphere correctly if we can't simulate the water vapor properly.

It is realized that most important mechanism to amplify the predicted global warming due to doubling of carbon dioxide is water vapor feedback [Manabe and Wetherald, 1967]. Recently, it has been suggest that the changes in the upper tropospheric moisture could significantly reduce the magnitude or even the sign of the water vapor feedback [Lindzen, 1990]. The distribution and supply of water vapor are the essential ingredients for our understanding of cloud distribution. Therefore, it is also crucial to the cloud feedback problem which comprises the largest uncertainty and causes different climate sensitivities among various climate general circulation models (GCMs) [Cess et al., 1990]. Proper assessment of moist processes is thus the fundamental requirement to simulate and understand the climate change.

Despite the importance of water vapor in the climate system, studies on the validation of water vapor climatology in the atmospheric GCMs are limited. Part of the reasons can attribute to the poor treatments of vapor advection scheme and uncertainties in formulating the source/sink of water vapor [Williamson and Rasch, 1994; Browning, 1994; Miller et al., 1992]. The shortcoming of observations further limits the attempt. The water vapor distribution is not well measured in the global scale. In particular, there are problems over the ocean, where the radiosonde humidity soundings are sparse and uneven, and in the upper troposphere where the radiosonde sensor is not very reliable [Chahine, 1992]. Fortunately, the extensive satellite archives in recent years provide alternative data sources for the water vapor and near-global coverage.

Soden and Bretherton [1994] have used the satellite observation to evaluate the spatial and temporal variations of total precipitable water (TPW) and the upper tropospheric humidity from the analyses of European Center for Medium-range Weather Forecasts (ECMWF) and the Community Climate Model (CCM) of National Center for Atmospheric Research. In their study, the retrieval of TPW is from the Special Sensor Microwave/ Imager (SSM/I) launched in 1987 on the operational spacecraft on the Defense Meteorological Space Program. It is considered more accurate than the retrieval from the previous microwave and infrared sensors [Liu et al., 1992]. The 6.7μm brightness temperature ($T_{6.7}$) from GOES is used as an indication for upper tropospheric moisture [Soden and Bretherton, 1993]. The ability of these models in simulating the primary features of the water vapor distribution is highlighted in their investigation. In this study, we follow the above comparison study with emphases on the water vapor climatology averaged from a longer term climate simulation. Also one of the major changes from the 3rd generation to 4th generation of the ECHAM model is the replacement of vapor advection scheme from the spectral method to the semi-Lagrangian transport algorithm [Williamson and Rasch, 1989]. The impacts of the advection scheme along with other changes in the parameterizations in the physical processes on the water vapor distribution are discussed. The satellite data used in this study and the characteristics of the ECHAM models are described in section 2. The comparison of the seasonal mean column integrated water vapor and

upper tropospheric humidity are presented in section 3 and 4, respectively. In the section 5, we briefly illustrate the impact of water vapor distribution simulation on model's energy budget and cloud distribution. Section 6 summaries the findings.

2. DATA

2.1 Satellite

2.1.1 SSM/I TPW

The TPW retrieval from SSM/I in this study uses the National Environmental Satellite Data and Information Service (NESDIS) algorithm [Alishouse et al., 1990]. Microwave TPW observations are generally considered to provide the best global measurements available. Uncertainties in the retrieved TPW are typically on the order of 2-3 kg/m^2 [Alishouse et al., 1990]. TPW is not retrieved over the land and ice covered ocean due to the large variation in surface emissivity. One advantage of the microwave retrieval is the availability under cloudy condition. Since our focus is on the evaluation of water vapor climatology, it is desirable to use the long term average from the observation for the comparison. An ensemble average of TPW from SSMI for the June, July, August (JJA) and December, January, February (DJF) seasons are derived from the data available between July 1987 to December 1992.

2.1.2 TOVS $T_{6.7}$

For the measure of moisture in the upper troposphere, the data from TIROS-N Operational Vertical Sounder (TOVS) in the NOAA operational polar-orbiting satellite are used [Wu et al., 1993]. Compared with similar measurements from GOES and METEOSAT, TOVS provides a better global coverage and a longer time span. The channel 12 (6.7 μm) of High-resolution Infrared Radiation Sounder (HIRS) unit in TOVS package is designed to sense the amount of water vapor in the upper troposphere. The sensitivity of HIRS channel 12 for a tropical temperature and moisture profile at nadir viewing is larger between 200 and 500 mb than other levels [Fig. 1 in Wu et al., 1993]. The overall error from instrument noise, angular correction, and cloud clearing for the brightness temperature at channel 12 is about 1 K for each pentad bin. One disadvantage for this data set is it has clear sky sampling bias. The magnitude of this bias is unknown [Wu et al., 1993].

The procedure for validating the distribution of upper tropospheric water vapor simulated by a GCM is to compare the observed clear-sky $T_{6.7}$ with that calculated by a radiative transfer model using GCM profiles of temperature and moisture as input. In this study, University of Wisconsin - Cooperative Institute for Meteorological Satellite Study (CIMSS) transmittance model is used to perform the $T_{6.7}$ calculation. The CIMSS research model is a 40-level, multivariate regression model based on FASCOD3 line-by-line transmittance calculations and is used also in Soden and Bretherton [1994]. The random error in the calculated brightness temperature is approximately 1-1.5 K. The seasonal and monthly means of $T_{6.7}$ are from ensemble average of data from all months between 1981 and 1989.

2.2 Models

TPW is directly taking from the model output and $T_{6.7}$ is calculated using the radiative transfer model described in the previous section.

Two versions of ECHAM model have the different advection schemes for water vapor and cloud liquid water. Though an idealized way of sensitivity study on the processes that determine the water vapor distribution would be that advection scheme are the only change involved. However, the 4th generation (newest version) of the atmospheric GCM in the Max-Planck Institute for Meteorology (ECHAM4) also involves many other changes with respect to previous version ECHAM3. Nevertheless, we will try to examine the differences in water vapor distribution in two models and trace the possible causes and impacts of the different parameterizations.

2.2.1 ECHAM3

The detailed description of the ECHAM3 is documented in a technical report from Max-Planck Institute for Meteorology [Roeckner et al., 1992]. The prognostic variables in the model include vorticity, divergence, temperature, surface pressure, water vapor and cloud water. The data used in this study is from a simulation with T42 resolution, 19 hybrid vertical levels. The finite difference representations of the vertical derivatives are of second order accuracy. Semi-implicit, leap frog time integration scheme with 24 minute time step is used. The seasonal climatological sea surface temperature (SST) and sea-ice from Atmospheric Model Intercomparison Project (AMIP) data set are used as surface boundary conditions.

The radiation scheme uses a broad-band formulation of radiative transfer equations with 6 spectral intervals in the infrared and 4 intervals in the solar part of the spectrum [Hense et al., 1982]. Gas absorptions due to water vapor, carbon dioxide, and ozone are included as well as scattering and absorption due to aerosols and

clouds. The single scattering properties and emissivity of cloud are parameterized in term of the predicted cloud liquid water and follow Stephens [1978].

The vertical turbulent transfer of momentum, heat, water vapor and cloud water is based on the Monin-Obukhov similarity theory for the surface layer and the eddy diffusivity approach above the surface layer [Louis, 1979]. The drag and heat transfer coefficients depend on roughness length and Richardson number, and the eddy diffusion coefficients depend on wind shear, mixing length and Richardson number which has been reformulated using cloud-conservative variables [Brinkop and Roeckner, 1993].

A mass flux scheme for deep, shallow, and mid-level convection is employed [Tiedtke, 1989]. Cumulus clouds are represented by a bulk model including the effect of entrainment and detrainment on the updraft and downdraft convective mass fluxes.

The prediction of stratiform clouds is based on the cloud water transport equation including sources and sinks due to condensation/evaporation, and precipitation formation by coalescence of cloud droplets and sedimentation of ice crystals [Sundquist, 1978; Roeckner et al., 1991]. Evaporations of cloud water and precipitation are considered. Sub-grid scale condensation and cloud formation is taken into account by specifying appropriate thresholds of relative humidity depending on height and stability [Xu and Krueger, 1991].

The land surface parameterization comprises the budgets of heat and water in the soil, the snow pack over land and the heat budget of permanent land ice and sea ice [Dümenil and Todini, 1992]. The heat transfer equation is solved in a 5-layer model with zero heat flux at the bottom. Soil moisture, vegetation, and snow are three reservoirs for the water budget equation. Vegetation effect such as interception of rain and snow in the canopy and stomatal control of evapotranspiration are parameterized [Blondin, 1989]. The runoff scheme is based on catchment considerations and takes into account sub-grid scale variations of field capacity over inhomogeneous terrain.

Seasonal averages of TWP and $T_{6.7}$ are derived from the ensemble monthly mean temperature and moisture profiles of a 20 year integration.

2.2.2 ECHAM4

It is known that moist filed has very large horizontal and vertical spatial variation. There are very strong and small scale sources and sinks of moisture associated with the phase changes. Thus, though the spectral transform method is a extremely good method for approximating large scale, global atmospheric dry dynamics, it does not have the same performance on the water vapor field [Rash and Williamson, 1991; Williamson and Rash, 1994]. One of the major changes from the ECHAM3 to ECHAM4 is that semi-Langrangian transport method [Williamson and Rash, 1989] replaces spectral method for the advection of moisture and cloud water. This has a potential to introduce significant changes in the water vapor distribution.

The new radiation code [Fouquart and Bonnel, 1980; Morcrette, 1991] is used with following modifications: (1) additional greenhouse gases (CH_4, N_2O, CFCs and 14.6 μm O_3 band) are included; (2) the single-scattering properties of cloud water droplets and ice-crystal are parameterized according to Rockel et al. [1991]. The effective radii of cloud droplets and ice crystals are parameterized from the liquid/solid water content, (3) the Viogt-line shape is used for the absorption line shape in the stratosphere [Giorgetta and Manzini, personal communication], (4) water vapor continuum is modified to include the temperature dependency of p-type continuum absorption [Giorgetta, personal communication].

The detrained fraction of the convective generated cloud water is coupled with stratiform (anvil) cloud water equation. The closure for the penetrative convection is changed from the moisture convergence to the buoyancy (CAPE) [Nordeng, 1994]. The first-order closure scheme for eddy diffusivity in the atmospheric boundary layer is replaced by a higher order turbulent kinetic energy closure with the Prandtl-Kolmogorov parameterization of eddy diffusivity [Brinkop and Roeckner, 1993].

A new global data set of land-surface parameters is used [Claussen et al., 1994]. These parameters including surface background albedo, surface roughness length, leaf area index, fractional vegetation cover, and forest ratio are constructed from the major ecosystem complex of Olson et al. [1983].

Seasonal averages of TWP and $T_{6.7}$ are derived from the ensemble monthly mean temperature and moisture profiles of a 10 year integration.

3. COLUMN INTEGRATED WATER VAPOR

3.1 TPW

The global distribution of the mean and seasonal variation of TPW from SSM/I observation, ECHAM3 and ECHAM4 are compared for the JJA (Fig. 1) and DJF (not shown) seasons. Comparison is done for only

the equatorward of 60° since the retrievals over the ice are less reliable.

The distribution of seasonal SSM/I are described in Liu et al. [1992] and Soden and Bretherton [1994]. Here we restate the distribution from a longer term average. The observed TPW fields from SSM/I are essentially zonal in nature, although variations along the latitude circle, generally associated with particular surface and large scale circulation features, are apparent. In tropics, there are variations related to the fluctuations of sea surface temperature, and therefore evaporation. For example the dry tongues along the west coast of the continents are likely related to the cold SST with ocean upwelling [Gaffen and Barnett, 1992]. The large scale atmospheric subsidences of dry air in these regions further suppress the water vapor abundance. The maximum TPW between 0 to 10 N along the latitude cycle highlight the location of the seasonal InterTropical Convergence Zone (ITCZ). The equatorial western Pacific warm pool region also show persistent greater TPW. The warmer SST and larger scale moisture convergence are the principle processes to enhance the TPW over this area. In JJA, the largest value of TPW are found over the Bay of Bengal, with area exceed 50 g/m^2 in TPW extended to India and south-east Asia. This maximum, reflects a mean convergence of low level moisture into this region, is an important part of the monsoon circulation. Much lower TPW are found in the mid-latitude, especially the winter hemisphere. This is expected from the latitudinal temperature gradient and the relation between temperature and saturation vapor pressure from the Clausius-Clapeyron equation. The seasonal cycle is more pronounced over the Northern Hemisphere. This is simply due to the moist air advect out from the continent interiors which have very large seasonal cycle of low level temperature.

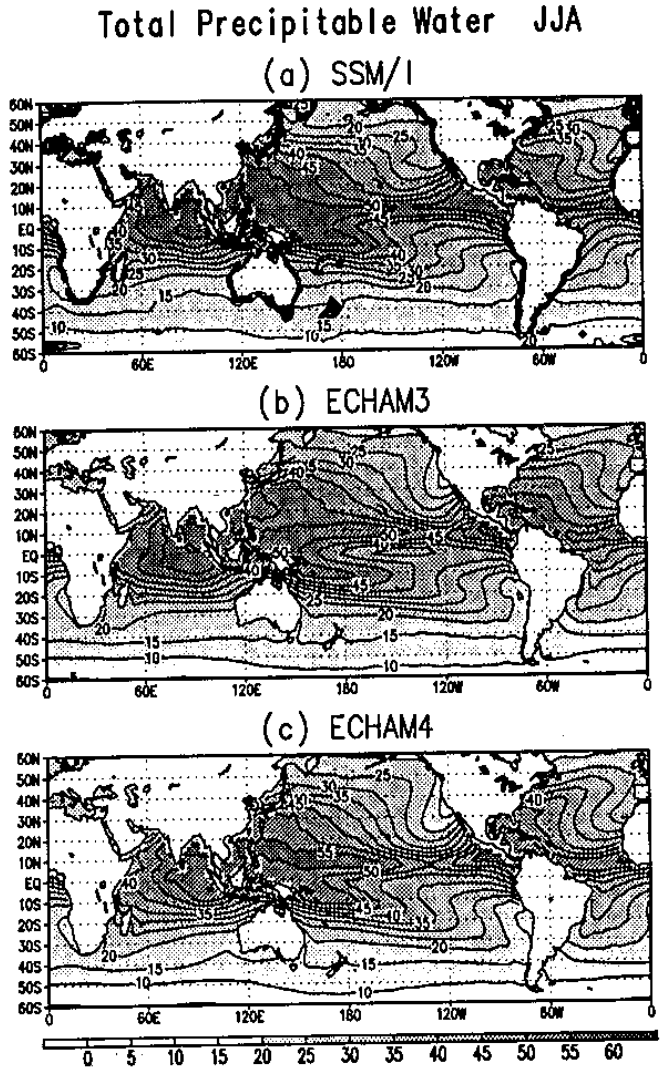

FIG. 1. The mean TPW from (a) SSM/I observations, (b) ECHAM3, and (c) ECHAM4 simulation for JJA. Units are kilograms per square meter.

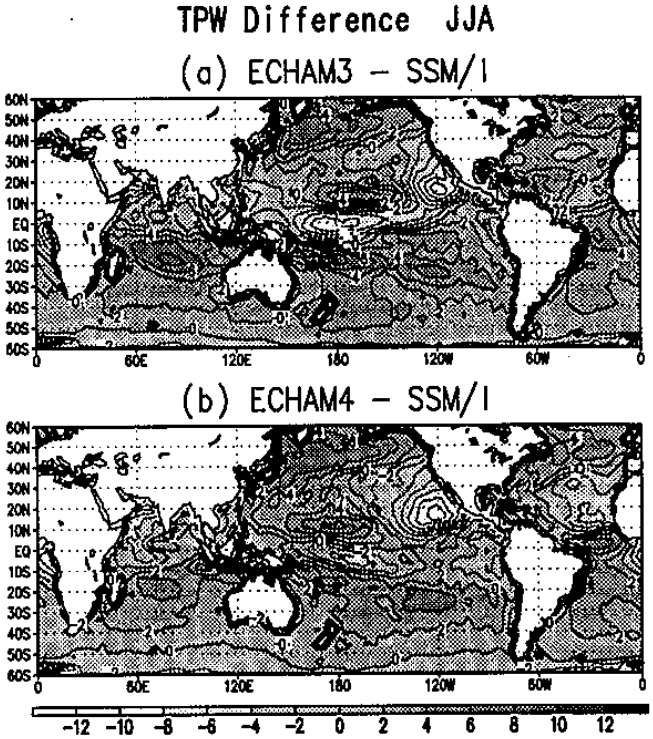

FIG. 2. Differences in TPW from (a) ECHAM3−SSM/I, and (b) ECHAM4−SSM/I for JJA.

The seasonal means and variations in TPW fields from ECHAM3 capture most the features described in the SSM/I observation. The location and movement of ITCZ, the summer time maximum at Bay of Bengal, the Pacific warm pool, and the extend of the dry tongues off the west coasts of continents are well simulated. Despite the overall good agreement, there are some systematic errors in TPW found in ECHAM3 (Fig. 2a). First, there is a drier (smaller TPW) zone consistently stay at central equatorial Pacific in both seasons. On the other hand,

the nearby convective centers are slightly more moist than the observation. The location of ITCZ and South Pacific Convergence Zone (SPCZ) are located slightly poleward in the model. There is a stronger separation of convection zone at west of dateline. This discrepancy is related the split ITCZ feature commonly found in the GCMs which uses moisture convergence closure for cumulus convection [Hess et al., 1993; Slingo et al., 1994]. Due to the Coriolis parameter, the frictional convergence can not maintained on the equator. Therefore with relatively uniform moisture in the lower troposphere, the deep convection would preferentially occur off the equator. In mid-latitude summer hemisphere, TPWs in ECHAM3 are greater than SSM/I observation, especially in the northern Pacific. The location of the dry tongue in the eastern subtropical Pacific are too strong and extend too further south. The comparison of mean sea level pressure from ECMWF analyses and ECHAM3 suggests the stronger subtropical high in the summer hemisphere are the primary reason for this east west discrepancy in TWP over the ocean basin. Similar discrepancy was also noted recently by Soden and Bretherton [1994] for a comparison between SSM/I and CCM2. There is also a tendency of broader latitudinal range for TPW > 30 kg/m^2 in the model. This suggests the Hadley circulation is extend more poleward. It has been illustrated that the Tiedtke's scheme generate a much broad deep convection heating and mean meridional circulation compared with a moisture adjustment scheme and available observational estimates [Slingo, 1994]. This broadening is also consistent with model bias of a more poleward subtropical jet and split ITCZ.

ECHAM4 simulation also capture the dominant feature of the mean and seasonal variation of TPW fields. TPWs over ITCZ, Pacific warm pool, dry tongue off the west coast of continents, and the maximum over the Bay of Bengal all have reasonable agreement with SSM/I. With different vapor advection schemes, deep convection closures and other changes, there is a improvement in TPW simulation in the equatorial region and winter hemisphere (Fig. 2b). The dry zone in the central Pacific is much less intense than ECHAM3. The position of the ITCZ and SPCZ are closer to the SSM/I observation indicated. This seems related with the new deep convection closure which do not preferentially form disturbances off the equator. However, the bias in the summer hemisphere ocean basin found in ECHAM3 is further enhanced. This bias is related to the additional problem in simulation the intensity of the subtropical high over the ocean in ECHAM4. The further enhanced anti-cyclonic circulation generate stronger dry-air-advection over the eastern half of the basins and moist-air advection over the western half. Part of the dry bias might be due to the stronger subsidence results from enhanced Hadley cell. Area of TPW > 30 g/m^2 is still greater than SSM/I observation. The problem of a broader range of Hadley circulation is remained in ECHAM4. The TPW in convection zones are greater in ECHAM4 than ECHAM3. It has been shown that the semi-Lagrangian scheme moistening the ascending branch of Hadley cell than that from the spectral method [Williamson and Rasch, 1994]. Also the drying in the descending branch extend to higher in the semi-Lagrangian version.

3.2 Normalized TPW parameter

Following the previous works [Prabhakara et al. 1979, Stephen, 1990; Soden and Bretherton, 1994], a normalized TPW parameter is used to illustrate the effect of large-scale circulation on the atmospheric water vapor distribution. Since the saturation water vapor pressure is depended on the temperature through the Clausius-Clapeyron relationship, the main pattern of the TPW reflect the thermodynamic influences from the SST. Therefore, it is not surprised to see the good agreements due to the prescribed climatological SST in the model run. Thus, it is more informative to show the dynamical impact through the normalized parameter. The normalized TWP parameter is defined as follows:

$$TPW^* = \frac{(TPW - TPW')}{TPW} \qquad (1)$$

which measures the relative contribution of dynamical influences to the TWP. Follow Soden and Bretherton [1994], TPW' in (1) is the total precipitable water estimated using a simplified model based on an approximate version of the Clausius-Clapeyron equation:

$$TPW' = 10.82\frac{r}{(1+\lambda)} exp\,(0.064\,(T_s - 288)) \qquad (2)$$

where T_s is the SST, r is the relative humidity and λ is the ratio of the atmospheric scale height to the scale height of water vapor and has a typical value of 3.5. The factor $r/(1+\lambda)$ is determined follow Soden and Bretherton [1994] using the regression between TPW from SSM/I and the right hand side of (2) using SST from National Meteorological Center. The value of this factor is equal to 0.178.

Fig. 3 illustrates the geographical distribution of seasonal mean TPW*, expressed as percentage, from SSM/I observation, ECHAM3 and ECHAM4 simulation. The positive TWP* means a grater than average moisture abundance for a specific SST. Thus, it is likely

to locate the region with moisture convergence or moist air advection. On the other hand, the negative value suggests the influence of subsidence or dry air advection. Both observation and the simulations from models show similar distributions of TPW* which highlight the impact from the large scale motions. The primary features in TPW* pattern are as follows: (i) negative values of TPW* are found for the areas of large scale subsidence off the west coast of continents; (ii) positive values of TPW* over the summer hemisphere midlatitude are consistent with the large northward flux of moisture by transient eddies. (iii) positive values of TPW* reflect the moisture convergence in ITCZ; (iv) the large negative values of TPW* over the winter hemisphere are associated with the descending branch of Hadley cell and the dry air advecting out from the colder continent. Although ECHAM3 qualitatively simulate most of the above features well, there are some biases as we already discussed in previous section. An advantage in the additional analyses here is that we gain more insight on the processes that are responsible for the biases. The moisture divergence in the central equatorial between the split ITCZ is not observed in SSM/I (Fig. 4a). The problem associated with moisture convergence closure is reaffirmed. The large scale subsidence and dry advection in the eastern subtropical Pacific are overestimated in JJA and extends further south. The continuing positive TPW* in ITCZ in JJA is slightly interrupted by this extension. The positive TPW* in mid-latitude summer hemisphere in ECHAM3 suggests an overestimate of moisture transport from low latitudes by transient eddies. The less negative TPW* in the winter hemisphere reveal that the air advect from continent is more moist than SSM/I observation suggested. The representation of slantwise and mid-level convections, common in midlatitude storm system, and their relations to the water vapor distribution also need further studies. One more problem is the dry air advection in the east of Japan and a similar but weaker dry feature in the east of Northern American continent in DJF. The dry advection zone in ECHAM3 are more poleward than SSM/I.

Most of those biases in mid-latitude are reduced in ECHAM4 (Fig. 4b). However, there are additional problems introduced. Though the split ITCZ feature is no longer persistent in the central equatorial Pacific, the moisture convergences (positive TPW*) are even stronger and broader than ECHAM3. The moisture convergence associated with SPCZ in DJF are extended toward south-east to the mid-latitude and much stronger than SSM/I observation. The east-west discrepancy in the

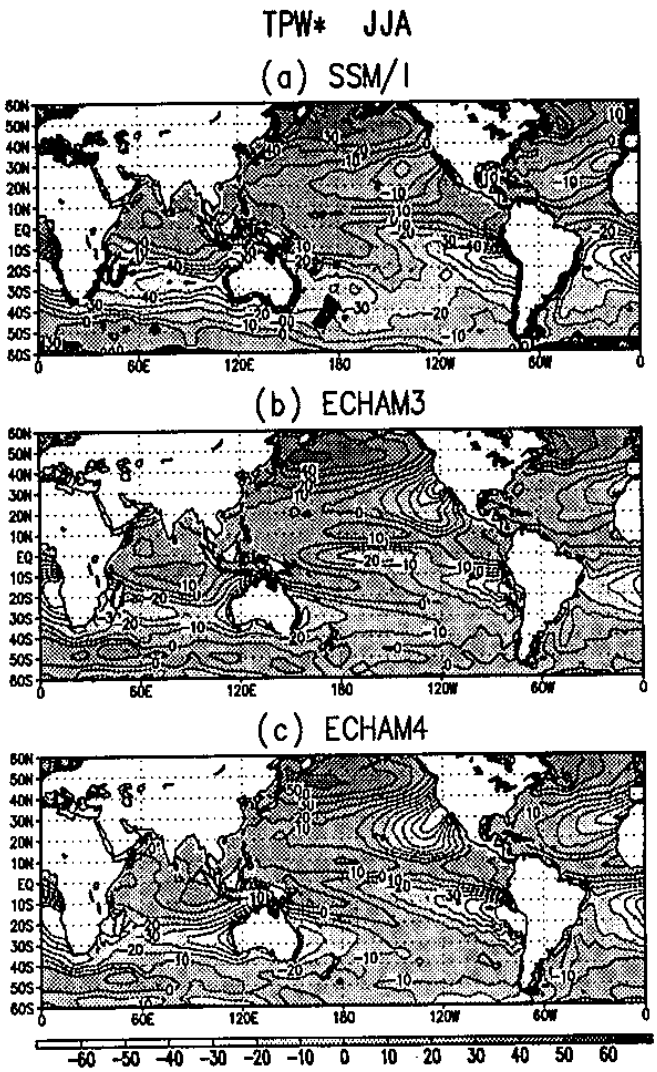

FIG. 3. Same as FIG.1, but for TPW*. Units are %.

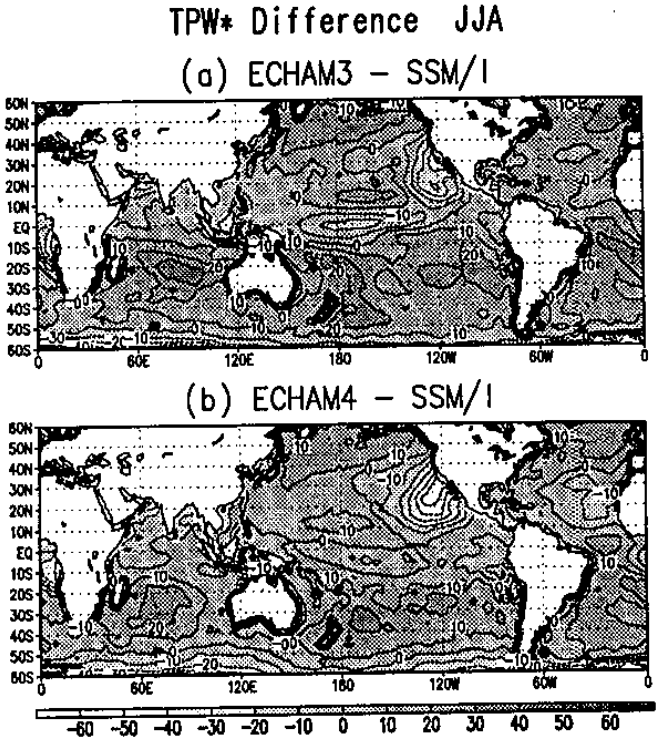

FIG. 4. Same as FIG.2, but for TPW*. Units are %.

summer hemisphere ocean basin associated with too intense subtropical high is further increased in ECHAM4.

4. MOISTURE IN THE UPPER TROPOSPHERE

Since the water vapor is concentrated in the first few kilometers above the ocean surface, the distribution of TPW is mainly the indication of the maritime boundary layer [Prabhakara et al., 1979]. We have outlined the importance of the upper tropospheric moisture in determining the amount of longwave radiation trapped by the atmosphere and it's implication in climate simulation. The upper tropospheric humidity is also important for simulation of the formation and dissipation of the high cirrus cloud. This again can significantly modify the terrestrial out-going longwave radiation and crucial to the earth's energy budget.

Here we use the $T_{6.7}$ measured from TOVS and calculated $T_{6.7}$ using the monthly mean temperature and moisture profiles from the model's long-term integration.

4.1 $T_{6.7}$

The geographical distribution of the mean and seasonal variation of $T_{6.7}$ from TOVS observation, ECHAM3 and ECHAM4 simulations are compared for JJA (Fig. 5) and DJF (not shown) seasons. The $T_{6.7}$ climatology is described in Wu et al. [1993]. Here we will reiterate the major features. The $T_{6.7}$ is primarily sensitive to relative humidity vertically averaged over a range of pressures in the upper troposphere. A higher $T_{6.7}$ indicates a drier upper troposphere unless there is a substantial temperature decrease. Note that the sensitivity of $T_{6.7}$ to moisture change is much larger than temperature change. The large scale subsidence makes the air warmer and drier, both the temperature and moisture make $T_{6.7}$ larger. The Convective activities, on the other hand, result slightly warmer and more moist upper troposphere. Thus, the response of $T_{6.7}$ to subsidence is greater than the convection.

There are apparent areas of drier upper troposphere corresponding to the descending branch of Hadley circulation and large scale subsidence coincide with the subtropical ridges off the west coast of continents in TOVS measurements. In JJA, the higher $T_{6.7}$ values are specially pronounced between 10 an 20 S from eastern Atlantic through the Indian Ocean, the eastern Pacific off Peru. There is another maximum over the northern Arabian Peninsula. This might be related to the extremely low amount of cirrus cloud in this region during boreal summer [Wu et al., 1993]. The eastern sub-

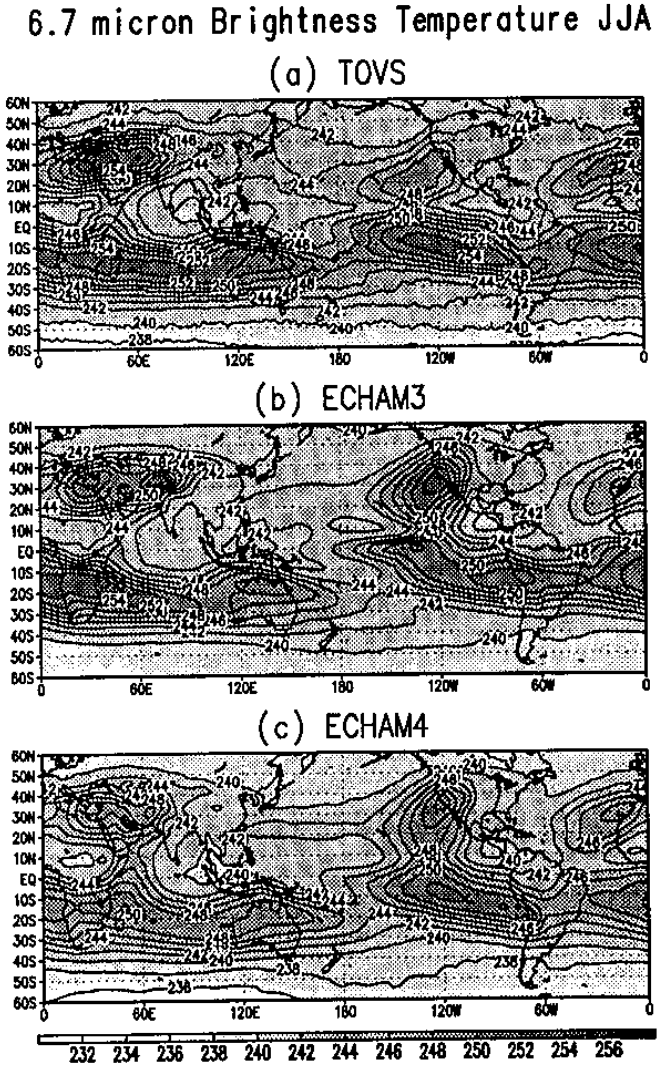

FIG. 5. The mean T6.7 from (a) TOVS observations, (b) ECHAM3, and (c) ECHAM4 simulation for JJA. Units are Kelvin

tropical Pacific and Atlantic Oceans in the Northern Hemisphere are not as dry as the aforementioned regions. The convection centers over the Pacific warm pool and Bay of Bengal, Central America and Africa have significant lower $T_{6.7}$. In DJF, the highest $T_{6.7}$ is found the central Pacific between 10 and 20 N. The low $T_{6.7}$ center in Central America moves to Brazil. The low $T_{6.7}$ center over Central Africa shift southward. The major low $T_{6.7}$ center over west Pacific and Indian Ocean also move southward and confined between equator and 10 S with a south-eastward extension. The location and seasonal variation of these low $T_{6.7}$ centers are well coincide with the climatology of the ITCZ [Waliser and Gautier, 1993]. It is evident that the upper tropospheric humidity is related to the penetrative convections. It has been argued that the upper-level clouds associated with convective updrafts are the major moisture source for the upper troposphere [Sun and Lindzen,

1993]. The locations of deep convective clouds categorized by International Satellite Cloud Climatology Project (ISCCP, Rossow and Lacis, 1990) are also resemble to the low $T_{6.7}$ centers.

ECHAM 3 qualitatively capture the pattern of high and low $T_{6.7}$ in both seasons successfully. However, there are some discrepancies. In JJA, the large scale subsidence off the west coast of North America in the model produces drier upper troposphere than TOVS observation (Fig. 6a). It suggests the simulated large scale subsidence in this region is too strong in the model. The areas between 10 and 20 S in the Indian Ocean and central Pacific are more moist in the ECHAM3. The range of the moist area in the equatorial convective region is larger than TOVS. Near the east coast of continents and west half of ocean basins in the Northern Hemisphere, $T_{6.7}$ is lower in the model. In DJF, The high $T_{6.7}$ zone in the central Pacific in ECHAM3 is not as strong as TOVS. The upper troposphere is drier off the west coast of continents, especially in the Southern Hemisphere. The range of low $T_{6.7}$ areas in the tropical region with more convective activities are larger in the model. These lower $T_{6.7}$ in the model also extend to the two major storm tracks. The biases are consistent with the previous described problems of a broader Hadley circulation and stronger vapor flux into midlatitude by transient eddies associated with storm tracks. One more noticeable difference is the dry upper troposphere in the model over the eastern Siberian and Sea of Okhotsk. This may related to the moisture advection scheme used in the model. We will show later that this bias is not found in ECHAM4. It should be noted that the observed $T_{6.7}$ could have systematic bias due to clear sky (dry) sampling. However, the observed $T_{6.7}$ values in tropics are subject to cloud contamination and lower the $T_{6.7}$. Detail error analyses are required to quantify the influences. For the subtropics, less sampling problem is introduced since the upper level cloud covers over these regions are rare.

ECHAM4 also capture the locations of high $T_{6.7}$ areas. However, it is generally showing higher relative humidities in the upper troposphere. In JJA, similar to ECHAM3, the major dry bias occurred in the region off the western coast of North America (Fig. 6b). This bias is slightly reduced compared to ECHAM3. There are other dry bias in the equatorial Indian Ocean and eastern equatorial Pacific. This suggests a stronger Walker circulation in ECHAM4. Thus, the enhanced subsidences (located at the descending branch of the east-west circulation along the equator) are shown with drier upper troposphere. The low $T_{6.7}$ centers over the convergence zone are again extend to a larger range than TOVS observation. The larger range of moist upper tropospheres region may cause by the broadening of the Hadley circulation in the model. The new moisture advection scheme in general has the effect to transport moisture to the upper troposphere in mid and high latitudes. Also the warm bias in the upper troposphere in ECHAM3 is reduced in ECHAM4. The reduction is mainly due to the changes in radiation code (we will not discuss this further here. It's to be described in a later paper). The combination of these two effects makes the upper troposphere relative humidity over the mid-latitude in ECHAM4 is higher than ECHAM3. In DJF, the low $T_{6.7}$ centers over the tropical convergence zones are again extend well beyond the TOVS observation indicates. This suggests the influence from a broader Hadley circulation in ECHAM4. There are also more moisture over the two major storm track. Another potential effect makes $T_{6.7}$ over convective centers and storm tracks in ECHAM4 lower than that in ECHAM3 is the increase of re-evaporation of cloud water. The coupling of the detrained cloud water from deep convection to the associated stratiform anvil cloud is introduced in ECHAM4. The dryness found over the eastern Siberian in ECHAM3 is no longer existed here. This is likely related with the vapor transport scheme change and reduction of warm bias mentioned earlier.

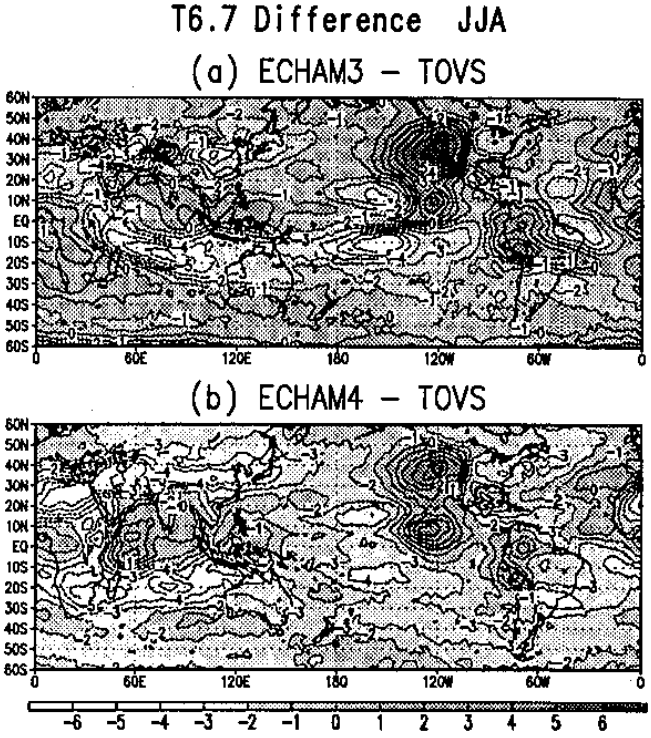

FIG. 6. Differences in T6.7 from (a) ECHAM3–TOVS, and (b) ECHAM4–TOVS for JJA.

4.2 Upper tropospheric humidity (UTH)

Although it is more appropriate to compare the observed and simulated $T_{6.7}$ in order to evaluate model's performance on the simulation of upper troposphere water vapor abundance, it is conceptually more clear if one can interpret the $T_{6.7}$ to a physical quantity. For this purpose, Soden and Bretherton [1993] developed an mean of interpretation based on a simplify treatment of the radiative transfer at 6.7 μm. They found that, accurate to about 1 K, the $T_{6.7}$ can be related to the relative humidity vertically averaged over the upper troposphere according to

$$\log\left(\frac{UTH \cdot P}{\cos\theta}\right) = a + b \cdot T_{6.7} \qquad (3)$$

where UTH is the weighted vertically average of upper tropospheric relative humidity, P is the pressure of T=240K divided by 300 mb, θ is the satellite zenith angle, and a = 31.50 and b=-0.1136 K^{-1} are regression coefficient. The typical value for P range from 0.9 to 1.5. The θ here is set to zero since the radiance measured by TOVS are 'limb-corrected' to produce the equivalent 'nadir-view" radiance [Wu et al., 1993]. The above formula is used to convert the $T_{6.7}$ to UTH.

The geographic distribution of the UTH inferred from $T_{6.7}$ of TOVS observation, ECHAM3, and ECHAM4 simulations are compared for JJA (Fig. 7) and DJF (not shown) seasons. In JJA, the moist convergence in Bay of Bengal bring the UTH over 70%. As we discussed in previous section, the areas with more convective activities, such as Central America and Africa, also have greater UTH. Convection and associated upper level cloud cover as the primary mechanism to transport the moisture to the upper troposphere is suggested. However, the formation and dissipation of the convective updraft and tropical cloud cluster, the associated precipitation processes, and how do they related to the UTH are still areas for further research [Betts, 1990; Sun and Lindzen, 1993]. There are also high UTH over the storm tracks. The vertical moisture advections and/or the re-evaporation from the upper level clouds generated by the mid-latitude synoptic systems are possible candidates for the high UTHs. The dry areas are mainly associated with the large scale subsidence over the descending branch of Hadley cell and eastern subtropical oceans. In DJF, the high UTH zones move southward and more limited than JJA. The major dry zones, on the other hand, moved to the Northern Hemisphere coincided with the shift of the downward branch of Hadley circulation. All these features have been indicated in $T_{6.7}$ distributions. Here we restate them in term of the more meaningful UTH.

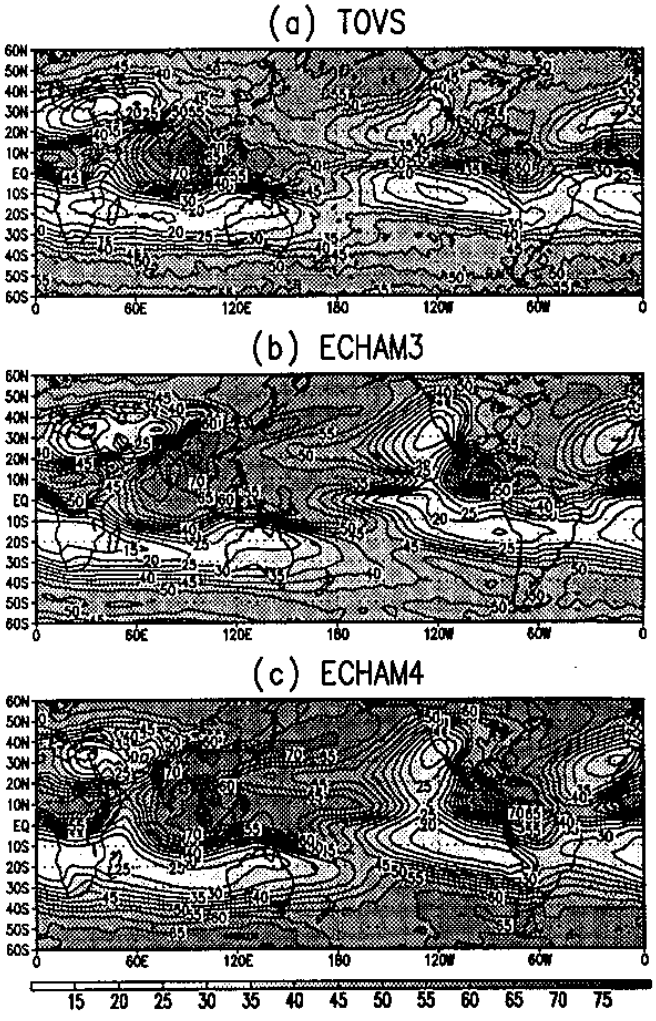

FIG. 7. Same as FIG. 5, but for UTH. Unit are %.

ECHAM3 successfully capture the major pattern of the mean and seasonal variation of UTH. As indicated in comparison of $T_{6.7}$, a much lower UTH is found off the west coast of North America in JJA (Fig. 8a). The high UTH in tropics extend to a larger area than TOVS. The maximum over Bay of Bengal is simulated well in the model with slightly more northward extension. The UTH in Central America is larger. The high UTH along ITCZ is suppressed near 120W. The problem of split ITCZ is clearly shown in the central Pacific with the two distinct high UTH. Also the storm track just east of Japan has higher UTH than TOVS. In DJF, the subtropical eastern oceans in Southern Hemisphere have lower UTHs. The mid-latitude continents are also too dry. The low UTH in the central Pacific is less intense. The high UTH in tropics tends to extend too further south in Southern Hemisphere.

The major features of UTH are reasonably simulated by ECHAM4. Some of the biases are described in

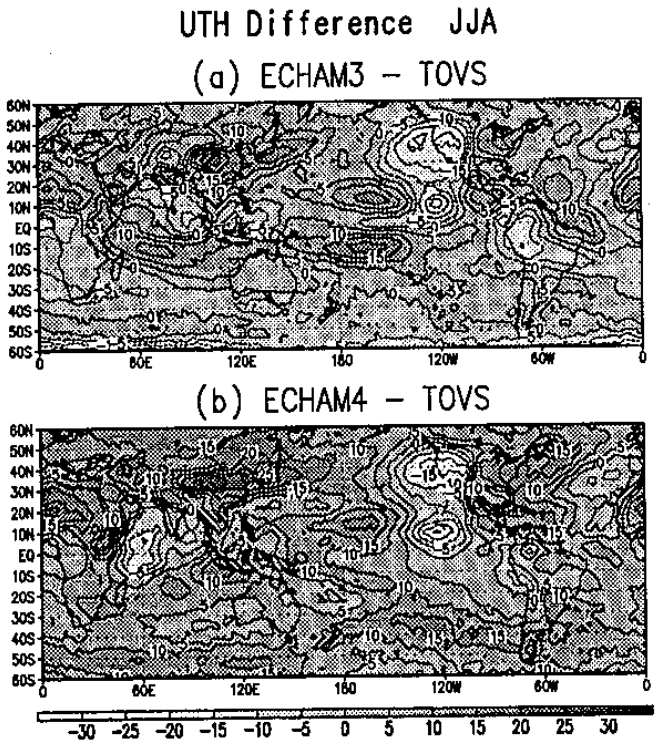

FIG. 8. Same as FIG. 6, but for UTH. Unit are %.

the following. In JJA, dry bias in UTH over the eastern subtropical ocean in ECHAM3 slightly reduced in ECHAM4 (Fig. 8b). The lower UTH in the descending region of Walker circulation highlight the overestimate of the strength of east-west circulation along the equator. All of the other places have generally higher UTH. The main convective region in tropics with maximum UTH covered a wider range than TOVS observation. There are also general increase of UTH in the midlatitude. This is related to the moisture increase due to the change of vapor advection scheme and the reduction of warm bias in upper troposphere. Largest moist bias in UTH are found in areas extend from central China to north Pacific. It is likely to associated with convective activities along the storm track. In DJF, lower UTHs are found in the eastern subtropical oceans. However, it's reduced compared to that in ECHAM3. The other major drier region is the northern Africa. The convective centers not only have higher UTH but also extend too further south. The moist biases associated with two storm tracks are larger in ECHAM4. The change in vapor advection scheme and reduction of the warm bias are again responsible for these larger UTHs.

We further illustrate the seasonal cycle of UTH. Fig. 9 shows the zonal mean UTH evolve in different months from TOVS, ECHAM3, and ECHAM4. The migration of ITCZ (higher UTH) and the subtropical dry zones (lower UTH) is clearly presented. The minimum UTH in the winter hemisphere subtropics highlight the intensification of the descending branch of Hadley cell. There is lags behind the solar heating cycle by approximately two months coincided with the migration of

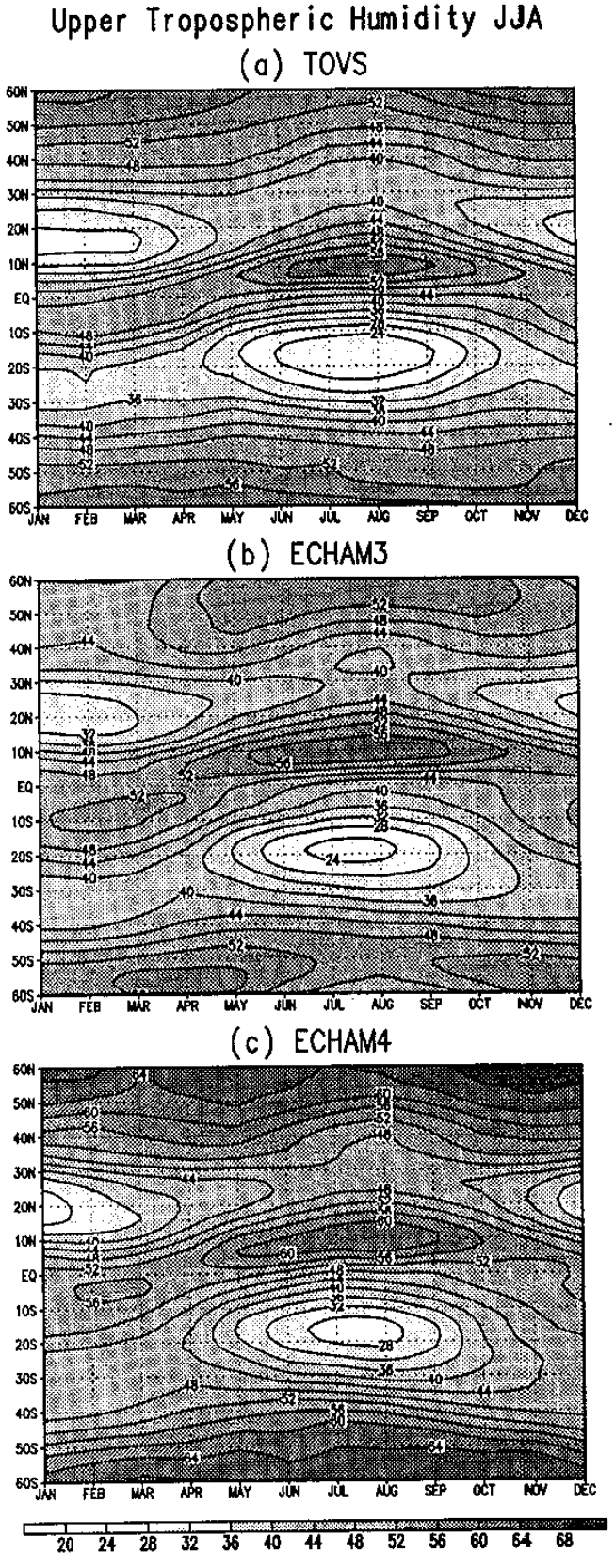

FIG. 9. Latitude-month distribution of the zonal mean UTH from (a) TOVS observation, (b) ECHAM3, (c) ECHAM4 simulations. Units are %.

ITCZ [Waliser and Gautier, 1993]. The seasonal variations of UTH in the midlatitude are larger in the Northern than in the Southern Hemisphere, as expected from the corresponding temperature variations. The differences in UTH between ECHAM3 and TOVS indicates the problems associated with UTH simulation (Fig. 10a). The broader latitude extent of higher UTH is related to the range of ITCZ. It suggests the convection scheme and the resulting split ITCZ could be the major contributors for this discrepancy. Recent studies [Hess et al., 1993; Slingo et al., 1994] have also illustrated the broad latitudinal extent characteristics of mean meridional circulation with Kou-type nad Tiedtke scheme. The seasonal variation of the UTH in the Northern Hemisphere mid-latitude seems to be out of phase from TOVS observation (or the UTH in northern winter is too low). This is mostly due to the spectral formulation of

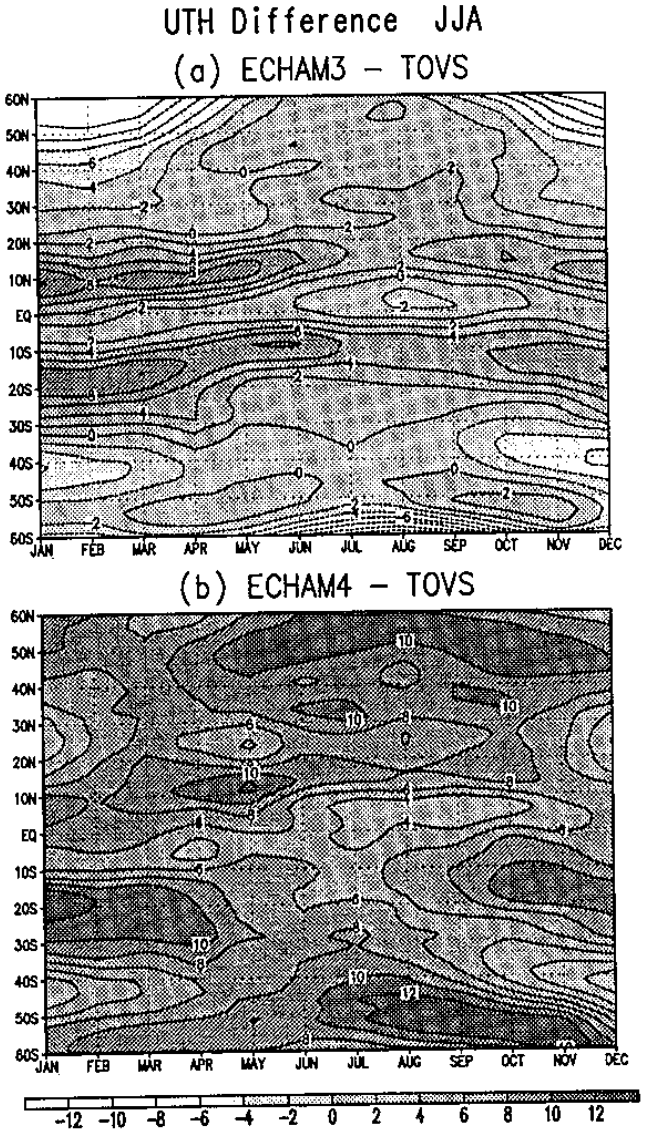

FIG. 10. Latitude-month distribution of the differences in zonal mean UTH from (a) ECHAM3–TOVS, and (b) ECHAM4–TOVS. Units are %.

vapor advection scheme failed to simulate the extremely low specific humidity in the upper troposphere of winter hemisphere at higher latitudes. Negative specific humidities are frequently found. On the other hand, the ECHAM4 show a general increase of zonal mean UTH almost everywhere (Fig. 10b). There is also problem of the broader latitudinal extent of higher UTH, especially DJF in the Southern Hemisphere. This is related to the rather strong strength of SPCZ in ECHAM4. The influence from the change in vapor advection scheme and reduction of warm bias on the UTH in the higher latitude is very significant. The UTH in these regions tend to be larger than TOVS observation. The more moist UTH has the consequence of increase high cloud cover. The re-evaporation/sublimation of the cloud water/ice can feed back as an additional increases in vapor sources.

5. IMPACT OF WATER VAPOR SIMULATION

In this section, we briefly discuss some of the problems in other aspects of model simulation which is influenced by the discrepancies in simulating water vapor distribution. One candidate for this is the clear sky outgoing longwave radiation (OLR) or greenhouse effect. An increase in water vapor will reduce the OLR and increase the greenhouse effect of clear sky, This effect should be more pronounced for the moisture in upper troposphere. Water vapor distribution also affects the cloud distribution since the cloud scheme used in model depends on the relative humidity.

5.1 Clear Sky greenhouse effect

Since the water vapor is the primary greenhouse gas with strong spatial variation, it is naturally to expect the abundance and vertical distribution of water vapor will strongly affect the clear sky greenhouse effect. We use a normalized greenhouse effect to examine the impact of water vapor distribution simulation on the model's radiation budget. The definition of the normalized clear sky greenhouse effect G_{clr} follow Stephens and Greenwald [1991]:

$$G_{clr} = \frac{\sigma T_s^4}{OLR_{clr}} \qquad (4)$$

where σ is the Boltzman constant, T_s is the surface temperature. In absence of the atmosphere, G_{clr} will be equal to one; the greenhouse effect of atmosphere leads to $G_{clr} > 1$. The OLR_{clr} is taking from the Earth Radiation Budget Experiment (ERBE, Barkstrom, 1984) measurements in clear sky condition. To avoid the land surface temperature which are calculated in models, we only look at the G_{clr} over the ocean. The prescribed SST

is used for all greenhouse effect calculations. Note that moisture differences in upper troposphere should have larger impact on the greenhouse effect than that in the lower troposphere. However, the differences in lower tropospheric water vapor are in general larger and their impact on the greenhouse effect can be as significant as UTH.

The geographic distribution of the mean G_{clr} from ERBE, and the differences in G_{clr} between ECHAM3, ECHAM4 and ERBE are shown for JJA (Fig. 11). The pattern of greenhouse effect from ERBE mainly follows the pattern of TPW observation. This is expected from the direct linkage between SST and OLR, and by inference column moisture [Raval and Ramanathan, 1989]. In ECHAM3, the biases near 10 S are associated with the split ITCZ simulated in the model. The moisture convergence and column precipitable water are overestimate over the region. Smaller G_{clr} off the west coast of the North America is resulted from both smaller TPW and UTH. The G_{clr} is even smaller over the region in ECHAM4 than that in ECHAM3. However, the biases associated with split ITCZ and broader Hadley circulation and, therefore, overestimate of G_{clr} near 10 S are slightly reduced. Nevertheless, there are still the enhancements of greenhouse effect in the tropics.

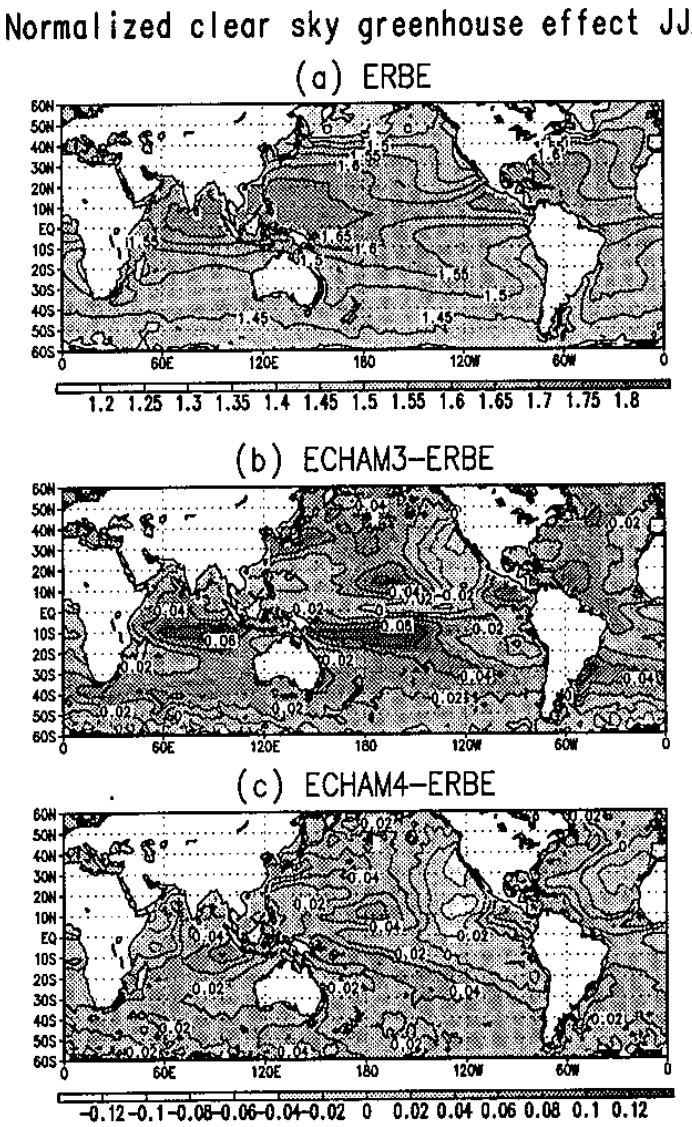

FIG. 11. Normalized clear sky greenhouse effect from (a) ERBE, and differences from (b) ECHAM3-ERBE, and (c) ECHAM4-ERBE for JJA.

5.2 Cloud distribution

The subgrid scale cloud formation is critically affected by the relative humidity predicted by model. However, the different cloud schemes along with other physical parameterizations can also have direct impact on the cloud amount [Slingo and Slingo, 1991]. We will limit the discussion to just highlight some of the model discrepancies in cloud simulation that could be related to the simulation of water vapor distribution. Since considerable discrepancies are found among observed cloud fields [Mokhov and Schlesinger, 1994], a reliable cloud climatology to test against the cloud vertical distribution is still not fully completed. Here we will use cloud radiative forcing from ERBE as a indication the possible problems in simulating the cloud fields and suggest the possible connection with the biases in water vapor distribution simulation in model.

Fig. 12 shows the difference in annual mean shortwave cloud radiative forcing between ERBE and ECHAM4. One of the problems is ECHAM4 tend to underestimate the shortwave cloud radiative forcing in the eastern subtropical ocean. This discrepancy is related to the low marine stratocumulus cloud amount simulated in model. There are indications of the larger cloudiness over those region from ground-based observation [Warren et al., 1988]. This underestimate of the cloudiness could be related to the dryness in the model. However, the realistic simulations of the atmospheric boundary layer, trade wind inversion along with the ade-

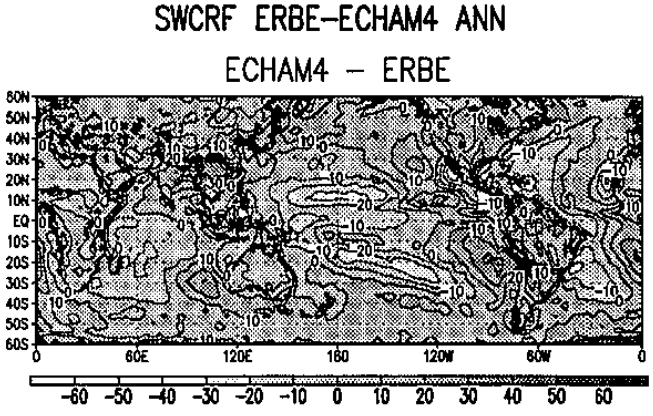

FIG. 12. Differences in the annual mean shortwave cloud radiative forcing from ECHAM4-ERBE. Units are Watts per square meter.

quate specification of the mixing, cloud formation and dissipation processes are also necessary.

6. SUMMARY

The satellite measurements provide unique new data sources for the water vapor distribution. There have been some developments of various means to interpret the measured radiance to the desired physical quantities and to illustrate the interaction with atmospheric circulation. Their application on the validation of the moist processes in climate model is invaluable since the traditional measurements reveal certain shortcomings. In this study, we show that the major features of geographical distribution and seasonal variation of the column moisture and relative humidity in the upper troposphere simulated in ECHAM models are comparable to those inferred from the satellite observations. Further, the comparisons between two version of ECHAM model highlight the impact from various changes in physical parameterization on the moisture fields.

The water vapor distribution, convergence and advection driven by the large scale circulation are reasonably well simulated in the models. However, there are apparent differences in the details. For the column moisture, both ECHAM3 and ECHAM4 have lower TPW over the eastern subtropical ocean in the summer hemisphere. This bias is introduced by both enhanced anticyclonic circulation associated with a stronger subtropical high and stronger subsidence over the region. The split ITCZ related to the deep convection closure and cumulus parameterization used in ECHAM3 leads to the dry bias in the central Pacific and the broadening of the Hadley cell. With different convection closure, this dry bias is less apparent in ECHAM4. The strength of Hadley and Walker circulation is intensified in ECHAM4 from ECHAM3. The higher TPWs in the convergence zones highlight this tendency. The increased radiation heating from the new radiation code, increased anvil cirrus cloud cover from the coupling of convective and stratiform cloud water, and increased moisture at convective centers using the new vapor advection scheme all interact in ECHAM4 through a positive feedback loop involving the radiative heating, latent heat release in convective cloud and moisture supply by the large scale dynamics and surface evaporation [Randall et. al., 1989].

For the moisture abundance in the upper troposphere, both ECHAM3 and ECHAM4 overestimate the range of higher UTH over the tropical convective centers. The impact from the broader Hadley cell is apparent and likely relates to the convective scheme. This bias is more intensified in ECHAM4 through the interactions among radiation, convection, and large scale dynamics resulting from various changes in physical parameterizations. The too intense Walker circulation is evident with the low UTH present in the subsidence region of the east-west longitudinal circulation at equator. Both models also overestimate the large scale subsidence off the west coast of continents in the summer hemisphere. UTH over the midlatitude in the winter hemisphere is too low, especially over the continents. The negative specific humidities results from the spectral transform method is the major reason for this dryness in ECHAM3. With new semi-Lagrangian advection scheme and reduction of warm bias in the upper troposphere, the UTH over these areas in ECHAM4 is no longer too dry and actually higher than that from TOVS observation. Whether the more moist upper troposphere over the midlatitude in ECHAM4 is due to greater upper level cloudiness, the water vapor transport scheme, or inefficient precipitation process is under investigation. It is also worth recalling that the TOVS measurement is subject to the clear sky (dry) sampling bias.

The discrepancies in simulating the water vapor distribution clearly affect the simulation of radiation budget. The greenhouse effect in the clear sky is overestimated over areas with higher TPW and UTH and vice versa. It is possible that the underestimate of the marine stratocumulus over the easter subtropical ocean is related to the dry bias in the model. However, the cloud scheme involves other macro-and-microphysical processes can be affected by other factors.

The evaluation of water vapor distribution from satellite observation provide an independent way to examine the dynamical and physical processes simulated in the model. A natural extension of this study is to formulate sensitivity study on the effect of various schemes on water vapor distribution. It would be interesting to study not only the mean fields but also the processes (e. g. aerial runoff) that contribute to the final water vapor distribution in these sensitivity study. However, the evaluation of the moist processes can be done only with the conventional radiosonde data.

7. REFERENCES

Alishouse, J., C. S. A. Snyder, J. Vongasthorn, and R. R. Ferraro, 1990: Determination of oceanic total precipitable water from the SSM/I, *IEEE Trans. Geosci. Remote Sens.*, **28**, 811-816.

Barkstrom B. R., 1984: The Earth Radiation Budget Experiment (ERBE), *Bull. Amer. Meteor. Soc.*, **65**, 1170-1185.

Betts, A. K., 1990: Greenhouse warming and the tropical water vapor budget. *Bull. Amer. Meteor. Soc.*, **71**, 1465-1467.

Blondin, C., 1989: Research on land surface parameterization schemes at ECMWF. *Proceedings of the workshop on "parameterization of fluxes over land surface"*, ECMWF, Reading, UK.

Brinkop, S., and E. Roeckner, 1993: Cloud-turbulence interactions: Sensitivity of a general circulation model to closure assumptions. *Max-Planck-Institüt für Meteorologie, Report No.* **117**, Hamburg 41pp.

Browning, K. A., 1994: Survey of perceived priority issues in the parameterizations of cloud-related processes in GCMs. *Q. J. R. Meteorol. Soc.*, **120**, 483-487.

Cess, R. D. et al., 1990: Intercomparison and interpretation of climate feedback processes in 19 atmospheric general circulation models. *J. Geophys. Res.*, **95**, 16601-16615.

Chahine, M. T., 1992: The hydrological cycle and its influence on climate. *Nature*, **359**, 373-380.

Claussen, M., U. Lohmann, E. Roeckner, and U. Schulzweida, 1994: A global data set of land-surface parameterization. *Max-Planck-Institüt für Meteorologie, Report No.* **135**, Hamburg 30pp

Dümenil, L. and E. Todini, 1992: A rainfall-runoff scheme for use in the Hamburg climate model. In: J. P. O'Kane (Ed.) *Advances in Theoretical hydrology, a tribute to James Dooge.* European Geophysical Society Series of Hydrological Sciences, 1. Elsevier.

Fouquart, Y., and B. Bonnel, 1980: Computations of solar heating of Earth's atmosphere: A new parameterization, *Beitr. Phys. Atmos.*, **53**, 35-62.

Gaffen, D. J. and T. P. Barnett, 1992: A comparison of observations and model simulations of tropospheric water vapor. *J. Geophys. Res.*, **97**, 2775-2780.

Hense, A., M. Kerschgens and E. Raschke, 1982: An economical method for computing radiative transfer in circulation models. *Q. J. R. Meteorol. Soc.*, **108**, 231-252.

Hess, P. G., D. S. Battisti, and P. J. Rasch, 1993: The maintenance of the intertropical convergence zones and the large scale tropical circulation on a water-covered earth. *J. Atmos. Sci.*, **50**, 691-713.

Lindzen, R. S., 1990: Some coolness concerning global warming. *Bull. Amer. Meteor. Soc.*, **71**, 288-299.

Louis, J. F., 1979: A parametric model of vertical eddy fluxes in the atmosphere. *Boundary Layer Meteorology*, **17**, 187-202.

Liu, T. W., W. Tang, and F. Wentz, 1992: Precipitable water and surface humidity over global oceans for the SSM/I and ECMWF, *J. Geophys. Res.*, **97**, 2251-2264.

Manabe, S., and R. T. Wetherald, 1967: Thermal equilibrium of the atmosphere with a given distribution of relative humidity, *J. Atmos. Sci.*, **24**, 241-259.

Miller, M. J., A. C. M. Beljaars, and T. N. Palmer, 1992: The sensitivity of the ECMWF model to the parameterization of evaporation from tropical oceans. *J. Climate*, **5**, 418-434.

Mokhov, I. I. and M. E. Schlesinger, 1994: Analysis of global cloudiness. 2. Comparison of ground-based and satellite-based cloud climatologies. *J. Geophys. Res.*, **99**, 17045-17065.

Morcrette, J.-J., 1991: Radiation and cloud radiative properties in the european centre for medium range weather forecasts forecasting system. *J. Geophys. Res.*, **96**, 9121-9132.

Nordeng, T. E., 1994: Extended versions of the convective parameterization scheme at ECMWF and their impact on the mean and transient activity of the model in the tropics. Submitted for publication in Q. J. R. Meteorol. Soc.

Olson, J. S., J. A. Watts, L. J. Allison, 1983: Carbon in live vegetation of major world ecosystems. ORNL-5862, Oak Ridge National Laboratory, Oak Ridge.

Prabhakara, C., G. Dalu, R. C. Lo, and N. R. Nath, 1979: Remote sensing of seasonal distribution of precipitable water over the oceans and the inference of boundary layer structure, *Mon. Wea. Rev.*, **107**, 1388-1401.

Rasch, P. J. and D. L. Williamson, 1991: The sensitivity of a general circulation model climate to the moisture transport formulation. *J. Geophys. Res.*, **96**, 13123-13137.

Raval, A. and V. Ramanathan, 1992: Observational determination of the greenhouse effect, *Nature*, **342**, 758-762.

Rockel, B., E. Raschke and B. Weyres, 1991: A parameterization of broad band radiative transfer properties of water, ice and mixed clouds. *Beitr. Phys. Atmos.*, **64**, 1-12.

Roeckner, E., M. Rieland and E. Keup, 1991: Modelling of cloud and radiation in the ECHAM model. *ECMWF/WCRP workshop on "clouds, radiative transfer and the hydrological cycle"*, 12-15 Nov. 1990, 199-222, ECMWF, Reading, UK.

Roeckner, E., K. Arpe, L. Bengtsson, S. Brinkop, L. Dümenil, M. Esch, E. Kirk, F. Lunkeit, M. Ponater, B. Rockel, R. Sausen, U. Schlese, S. Schubert, M. Windelband, 1992: Simulation of the present-day climate with the ECHAM model: Impact of model

physics and resolution. *Max-Planck-Institüt für Meteorologie, Report No.* **93**, Hamburg 171pp.

Rossow, W. B. and A. A. Lacis, 1990: Global, seasonal cloud variation from satellite radiance measurements. part II: cloud properties and radiative effects, *J. Climate.*, **3.**, 1204-1253.

Slingo, A. and J. M. Slingo: 1991: Response of the National Center for Atmospheric Research community climate model to improvements in representation of clouds, *J. Geophys. Res.*, **96**, 15341-15357.

Slingo, J. M., M. Blackburn, A, Betts, R. Brugge, K. Hodges, B. Hoskins, M. Miller, L. Steenman-Clark, and J. Thuburn, 1994: Mean climate and transience in the tropics of the UGAMP GCM: Sensitivity to convective parameterization. *Q. J. R. Meteorol. Soc.*, **120**, 881-922.

Soden, B. J., and F. P. Bretherton, 1993: Upper tropospheric relative humidity from the GOES 6.7-μm channel: Method and climatology for July 1987, *J. Geophys. Res.*, **98**, 16669-16688.

Soden, B. J., and F. P. Bretherton, 1994: Evaluation of water vapor distribution in general circulation models using satellite observation. *J. Geophys. Res.*, **99**, 1187-1210.

Stephens, G. L., 1978: Radiation profiles in extended water clouds: 2. parameterization schemes. *J. Atmos. Sci.*, **35**, 2123-2132.

Stephens, G. L., 1990: On the relationship between water vapor over the ocean and sea surface temperature. *J. Climate.*, **3**, 634-645.

Stephens, G. L. and T. J. Greenwald, 1991: The earth's radiation budget and its relation to atmospheric hydrology. 1. Observations of the clear sky greenhouse effect. *J. Geophys. Res.*, **96**, 15311-15324.

Sun, D.-Z., R. S. Lindzen, 1993: Distribution of tropical tropospheric water vapor. *J. Atmos. Sci.*, **50**, 1643-1660.

Sundquist, H., 1978: A parameterization scheme for non-convective condensation including prediction of cloud water content. *Q. J. R. Meteorol. Soc.*, **104**, 677-690.

Tiedtke, M. 1989: A comprehensive mass flux scheme for cumulus parameterization in large scale models. *Mon. Wea. Rev.*, **117**, 1779-1800.

Waliser, D. E., and C. Gautier, 1993: A satellite-derived climatology of the ITCZ. *J. Climate.*, **6**, 2162-2174.

Warren, S. G., C. J. Hahn, J. London, R. M. Chervin, and R. L. Jenne, 1988: *Global distribution of total cloud cover and cloud type amounts over ocean.* NCAR/TN-317+STR, 40pp., 170 maps.

Williamson, D. L., and P. J. Rasch, 1989: Two dimensional semi-Lagrangian transport with shape preserving interpolation. *Mon. Wea. Rev.*, **117**, 102-129.

Williamson, D. L., and P. J. Rasch, 1994: Water vapor transport in the NCAR CCM2. *Tellus*, **46A**, 34-51.

Wu, X., J. J. Bates, S. J. S. Khalsa, 1993: A climatology of the water vapor band brightness temperatures from NOAA Operational satellites. *J. Clim*ate., **6**, 1282-1300.

Xu, K. M., and S. K. Krueger, 1991: Evaluation of cloudiness parameterization using a cumulus ensemble model. *Mon. Wea. Rev.*, **119**, 342-367.